Received: 27 February 2021 | Revised: 21 April 2021 | Accepted: 2 May 2021

DOI: 10.1002/jrs.6141

SPECIAL ISSUE - RESEARCH ARTICLE

Journal of RAMAN SPECTROSCOPY WILEY

Vibrational study of lead bromide perovskite materials with variable cations based on Raman spectroscopy and density functional theory

Supriya Ghosh[1] | **Debkumar Rana**[1] | **Bapi Pradhan**[2] | **Patrice Donfack**[1] | **Johan Hofkens**[2,3] | **Arnulf Materny**[1]

[1]Department of Physics and Earth Sciences, Jacobs University Bremen, Bremen, Germany

[2]Department of Chemistry, KU Leuven, Heverlee, Belgium

[3]Max Planck Institute for Polymer Research, Mainz, Germany

Correspondence
Arnulf Materny Department of Physics and Earth Sciences, Jacobs University Bremen, Campus Ring 1, 28759, Bremen, Germany.
Email: a.materny@jacobs-university.de

Funding information
Alexander von Humboldt-Stiftung, Grant/Award Number: Ref 3.5 - 1205997 - IND - HFST-P; Max-Planck-Gesellschaft, Grant/Award Number: MPI Fellow; Onderzoeksraad, KU Leuven, Grant/Award Number: iBOF-21-085 PERSIST; Vlaamse regering, Grant/Award Numbers: CASAS2, Meth/15/04; Fonds Wetenschappelijk Onderzoek, Grant/Award Numbers: 1275521N, G0A5817N, G098319N, W002221N, S002019N, ZW15_09-G0H6316N

Abstract

Metal halide-based perovskite semiconductors exhibit excellent optoelectronic properties such as a sharp absorption edge, high absorption coefficients, and a small recombination rate. Mixed compositions result in a variation of the structure of these perovskite materials, which also influences their electronic properties. Even though huge progress in synthesis and device fabrication has been made, still systematic investigations of structural properties of lead halide-based perovskites are missing. Here, we systematically investigate the vibrational features of lead bromide-based perovskites using Raman spectroscopy and density functional theory (DFT). We have performed these investigations using MA^+, FA^+, and Cs^+ as cations in the lead bromide structures and determined the vibrational modes both from Raman experiments and DFT simulations. We find a clear dependence of the Raman band wavenumbers on the chosen cations. The structural differences are reflected in the different line-width broadening of Raman bands, charge distribution on the cations and the extent of their interactions with the bromide anions.

KEYWORDS
density functional theory (DFT), perovskites, Raman spectroscopy

Debkumar Rana and Bapi Pradhan contributed equally.

This paper is dedicated to late Prof. Derek A. Long whose important works in the field of Raman spectroscopy contributed fundamentally to the development of this technique.

1 | INTRODUCTION

Metal halide perovskites (MHP), in particular the tri-halide perovskites, are a remarkable class of materials that have resulted in a rapid series of breakthroughs in the field of optoelectronic devices.[1–6] Over the past decades the MHPs have emerged as suitable materials for solar cells, light emitting diodes, lasers, transistors, and memory devices.[7–13] It has been demonstrated that MHP-based photovoltaic devices show power conversion efficiencies of more than 22%,[14,15] and the devices can be produced on cheap non-crystalline substrates by both vapor deposition and solution processing.[8,11,16,17] Their excellent performance originates from the outstanding optoelectronic properties such as direct band-to-band recombination, long exciton diffusion length, high absorption coefficient. and long photoluminescence (PL) lifetime.[9,18–20]

MHPs are characterized by the general chemical formula ABX_3, where A is an organic or inorganic cation (methylammonium (MA), formamidinium (FA), or cesium (Cs)), B = Pb^{2+} or Sn^{2+}, and X is a halide anion (Cl^-, Br^-, and I^-, or an alloyed combination of these). The change of A and B sites in MHP influences lattice dynamics, phase transitions, and the interactions between the organic and inorganic counterparts. Infrared and Raman spectroscopy have proven to be very useful for studying properties of hybrid perovskite materials. Following reports of highly efficient solar cells fabricated with $MAPbI_3$, many infrared[21–23] and Raman studies have been performed.[24–28] For example, Raman spectroscopy can be used for in situ studies of devices fabricated on a glass substrate; that is, buried layers. Low-wavenumber lattice vibrations can also be detected by Raman spectroscopy. Indeed, it was shown that scattering from longitudinal optical phonons via the Fröhlich interaction dominates electron scattering at room temperature in double perovskites, manifested within the nominally non-resonant Raman spectrum as multi-phonon processes up to the fourth order.[29] As a further example, surface structural changes that go hand in hand with perovskite decomposition upon light irradiation have been characterized by Raman spectroscopy.[30]

Despite high power conversion efficiency, the development of MA-based perovskite devices is plagued by their poor resistance to moisture or high temperatures, as well as by the formation of trap states induced by the exposure to light.[31,32] In principle, the synthesis of $FAPbX_3$ provides an attractive alternative as it has a band gap smaller than its MA counterpart.[11,33] It influences the device conversion efficiency, as the bandgap is closer to the optimal value for a single junction solar cell.[34] Alternatively, fully inorganic cesium-based $CsPbX_3$ perovskite compounds have excellent thermal stability up to 450°C and they have been explored as efficient light harvesters.[15,35] $MAPbX_3$, $FAPbX_3$, and $CsPbX_3$ represent prototype systems for photovoltaic applications. The structures and properties of these materials have been investigated by X-ray diffraction and UV–Vis spectroscopy, along with electronic structure calculations.[36–39] However, a comprehensive vibrational spectroscopic study of $MAPbBr_3$, $FAPbBr_3$, and $CsPbBr_3$, particularly, a comparative study of the effect of different cations on the vibrational relaxation process is still missing.

Here, we report a combined experimental and theoretical Raman vibrational analysis of $MAPbBr_3$, $FAPbBr_3$, and $CsPbBr_3$ perovskites in both low- and medium-wavenumber region, where the bands associated with the vibrations of the interacting inorganic and organic constituents are expected. The cubic structures of these three materials are shown in Figure 1. The assignment of the Raman spectral features of $MAPbBr_3$ (MPB), $FAPbBr_3$ (FPB), and $CsPbBr_3$ (CPB) is supported by first-principles DFT calculations carried out on simplified models. We have analyzed the changes in Raman bandwidths and peak positions in detail, focusing our attention on the intramolecular vibrations of different organic cations.

This paper is dedicated to late Prof. Derek A. Long. His pioneering work in the field of Raman spectroscopy contributed significantly to the great popularity of this method in different areas of research. His well-known book on Raman spectroscopy[40] still serves as reference for many researchers. An overview about his many contributions to the development and use of this technique can, for example, be found in the appreciation of Prof. Long's work by Edwards.[41]

2 | EXPERIMENTAL DETAILS

2.1 | Synthesis of CsPbBr3, MAPbBr3, and FAPbBr3 microcrystals

$PbBr_2$ (99.99%) was purchased from Sigma-Aldrich, CsBr (99.99%) was obtained from Alfa Aesar, hydrobromic acid (48 wt. % in H_2O) was purchased from Acros Organics, and formamidinium bromide (FABr) and methylammonium bromide (MABr) salts were obtained from Greatcell Solar Materials. All the chemicals were stored under inert argon atmosphere and used without further purifications.

$CsPbBr_3$: For the synthesis of **$CsPbBr_3$** microcrystals, 10.1 mmol $PbBr_2$ (3.7 g) was dissolved in 8 ml of concentrated hydrobromic acid, and 10 mmol CsBr (2.12 g) was dissolved in 2-ml water by prolonged sonication. Then, the CsBr solution was added to the $PbBr_2$ solution swiftly,

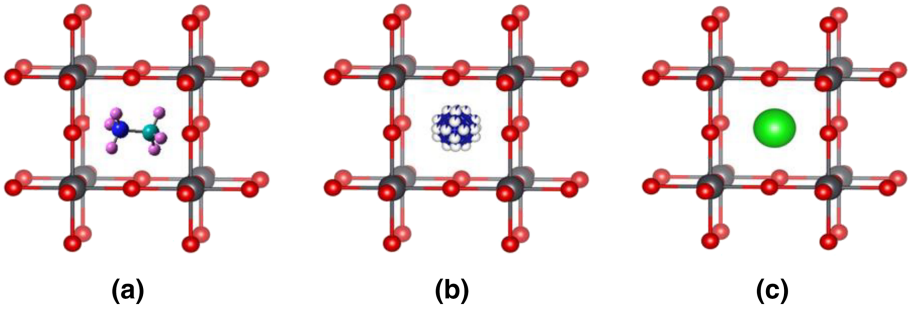

FIGURE 1 Structures of lead bromide-based perovskites (a) $MAPbBr_3$, (b) $FAPbBr_3$, and (c) $CsPbBr_3$

resulting in immediate formation of $CsPbBr_3$ microcrystals. The mixture was left for 2 h at room temperature under magnetic stirring. The filtrated microcrystals were washed twice with diethyl ether followed by vacuum drying for further use.[3]

$MAPbBr_3$: For the synthesis of **$MAPbBr_3$** microcrystals, 2 mmol of $PbBr_2$ (734 mg) and 2 mmol of MABr (224 mg) were dissolved in 6 ml of solvent mixture of dimethylformamide and γ-butyrolactone (DMF:GBL) (4:2 v/v) at room temperature under stirring. The solution was filtered using a 0.22-μm pore size filter, followed by dilution in 6-ml DMF. Twenty-milliliter toluene was added to saturate the solution. Orange colored $MAPbBr_3$ microcrystals were formed after stirring on a hot plate at 80°C for 10 min. The particles were filtered and washed with toluene followed by vacuum drying for further use.[42]

$FAPbBr_3$: For the synthesis of **$FAPbBr_3$** microcrystals, 5 mmol of $PbBr_2$ (1.835 g) and 5 mmol of FABr (625 mg) were dissolved in a 10-ml mixed DMF:GBL (1:1 v/v) solvent at room temperature under stirring. To remove impurities and non-dissolved salts, the solution was filtered using nylon filters with a 0.22-μm pore size. The filtrate was diluted in 20-ml DMF. Then, 40 ml of toluene was added to the filtrate followed by 80°C hearing on a hot plate with 400 rpm stirring for 40 min. The microcrystals were filtered, washed with toluene and vacuum dried for further use.[43]

2.2 | Spectroscopic techniques

2.2.1 | UV–Vis absorption and photoluminescence

For all optical measurements, the microcrystal particles from each sample dispersed in hexane were drop-cast on a cover slip and let to dry at room temperature. UV–Vis absorption and photoluminescence (PL) spectra were taken using a Perkin Elmer Lambda 950 and an Edinburgh FLS980 spectrometer, respectively.

2.2.2 | Raman spectroscopy

A portable i-Raman Plus spectrometer (BWS465-785S, B&W Tek, USA) was used for Raman measurements. It features an easy-to-use fiber-coupled and compact Raman spectrometer with built-in parts including a detector, a near-infrared 785-nm laser source for excitation, and a fixed grating allowing a very wide spectral coverage up to 3350 cm^{-1} within a single detection window. In addition, the system is equipped with an optical fiber probe with an actual Raman cut-off at 47 cm^{-1} (better than the system specification). This allows low-wavenumber Stokes Raman shift detection as close as 65 cm^{-1} (the low Raman spectral range specification) or less from the laser line. The optical fiber probe head of the laser is optionally fitted into a narrow collimator lens tube in order to couple it with a compact microscope assembly, which enables detailed analysis through a microscope objective. This combination, including a ×50 long working distance microscope objective with 0.50 numerical aperture, resulted in a beam spot size of 30–35 μm on the sample. All spectra were recorded in the 180° back scattering geometry. The system delivers a spectral resolution of about 4 cm^{-1}. The aromatic ring breathing mode of toluene at 1003.7 cm^{-1} was used for checking the wavenumber calibration of the system. The BWSpec Software (version 4.03_33, B&W Tek, USA) was used to control the i-Raman Plus spectrometer and to automatically monitor the laser power delivered to the sample.

3 | COMPUTATIONAL DETAILS

All quantum chemical calculations have been carried out using the Gaussian 09 software package.[44] The ground state structures of the cation-anion systems, i.e., $CH_3NH_3Br_3$ ($MABr_3$), $CH_3NH_2Br_3$ ($FABr_3$), and $CsBr_3$ have been optimized using density functional theory (DFT) with the LSDA functional and LanL2DZ basis set. The separated cations, that is, $CH_3NH_3^+$ and

$CH_3NH_2^+$ have been also optimized using the B3LYP functional and LanL2DZ basis set. The optimized structures are shown in Figure 2. The optimized energies are given for all the cases in Table S1 showing how the single crystals differ from the whole compounds. In addition, we also present the coordination bond lengths for each case in Figure 2.

The same basis sets have been used to calculate the vibrational wavenumbers along with the Raman band intensities. For all cases, the optimized geometries and structures converged to the minima of the potential energy surfaces; no negative wavenumbers resulted from the wavenumber calculations. To analyze and visualize the data, the GaussView 5 software has been used.[45] Quarti et al.[24] demonstrated that comparing the simplified structure MAI_3 with the complete periodic structure $MAPbI_3$, the vibrational features remained nearly unchanged. This can also be expected for our system. Therefore, we have concentrated on the calculation of Raman spectra for the isolated parts of each material under consideration and compared them with the experimental Raman spectra. With this, we obtain the desired information about the influence of the different cations on the vibrational and thus structural properties of the bulk perovskite material, which up to now was missing.

4 | RESULTS AND DISCUSSION

Figure 3 shows the electronic absorption and emission spectra as well as powder X-ray diffraction (XRD) patterns of MPB, FPB, and CPB perovskites. The absorption peak positions are 519, 517, and 516 nm for FPB, MPB, and CPB, respectively. The PL peak positions are 564, 534, and 531 nm for FPB, MPB, and CPB respectively. The XRD results confirmed the cubic phase of the FPB and MPB, and the orthorhombic phase of the CPB perovskites.[39,42,46] The energy bandgap increases from FPB to CPB due decreasing dielectric constant of the A site cation, which in consequence results in an increase of the exciton binding energy.[35] The small Stokes shift between absorption and emission peaks indicates, that the PL originates from band edge states. To avoid laser-induced degradation during measurement, we have selected an optical excitation wavelength of 785 nm for the Raman spectra measurements.

The Raman spectra were measured from FPB, MPB, and CPB powder samples. The spectra are analogous to those reported earlier for perovskite samples.[35,47,48] In our work, we compare three samples by using a combination of Raman spectroscopy and DFT. Figures 4–6 show parts of the Raman spectra obtained from MPB, FPB, and CPB, respectively. The spectrum of MPB shows different

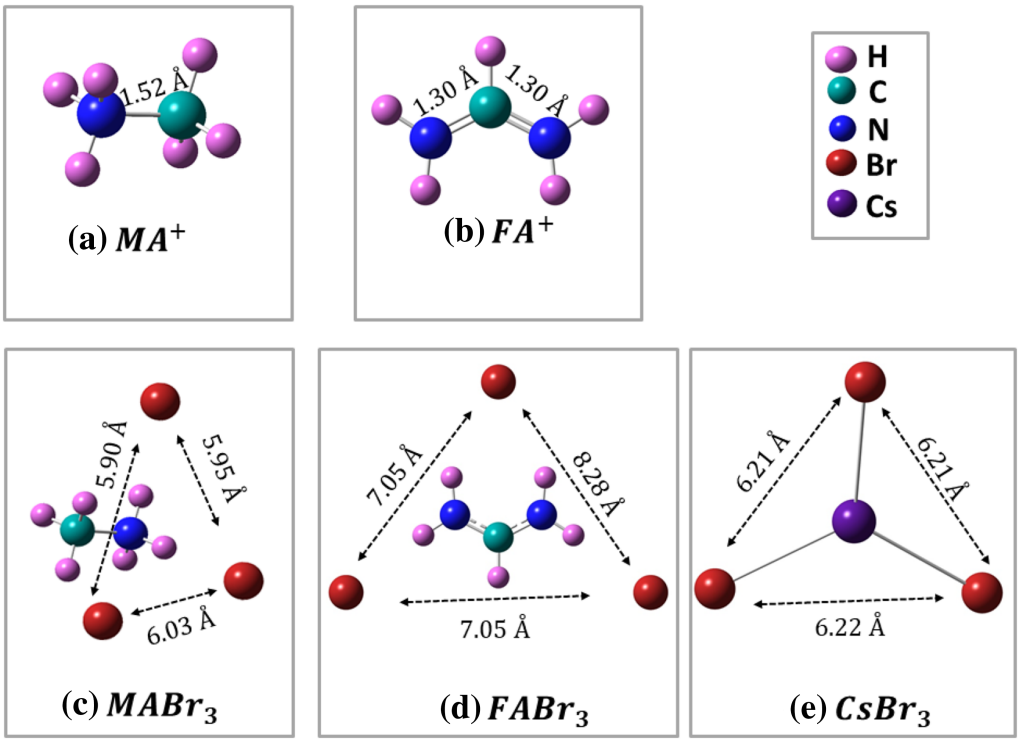

FIGURE 2 Optimized structures of different parts of lead bromide-based perovskites (a) MA^+, (b) FA^+, (c) $MABr_3$, (d) $FABr_3$, and (e) $CsBr_3$. The coordination bond lengths are also shown for each case

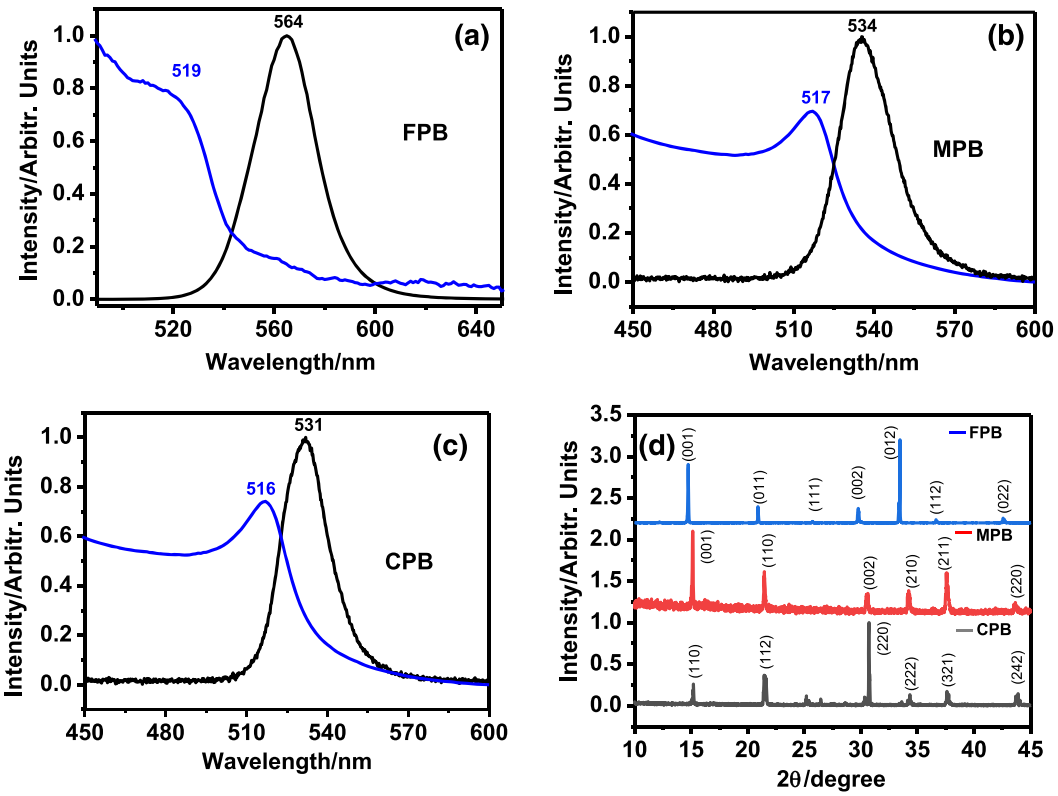

FIGURE 3 Electronic absorption (blue) and emission (black) spectra of (a) FPB, (b) MPB, (c) CPB perovskites, and (d) respective powder X-ray diffraction (XRD) patterns

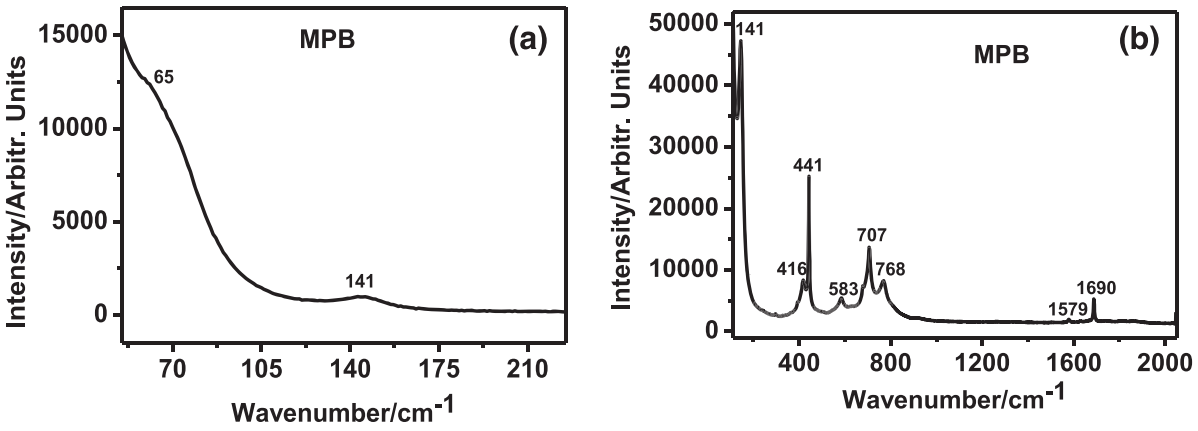

FIGURE 4 Raman spectra of MPB in the (a) low- and (b) medium-wavenumber region

vibrational bands in the low wavenumber region. The Raman signals at 65 and 141 cm^{-1} are in good agreement with results reported in previous literature.[24] The band at 65 cm^{-1} is mainly due to the bending mode of the Br-Pb-Br bonds. The presence of the 65 cm^{-1} band also in CPB (see Figure 6) confirms that this band is associated to the inorganic cage. The band at 141 cm^{-1} is due to the liberation of cations involving the deformation of the inorganic cage.[24] The band falling in the range between 400 and 450 cm^{-1} in MPB is mainly determined by the torsional motion of the MA cations.[24,27,49] This is confirmed by the absence of this band in CPB. The band observed in the range 700–800 cm^{-1} can be assigned to MA rocking (both CH_3 and NH_3^+ rocking), which is sensitive to the phase transition of MPB.[28]

For a better assignment of the Raman modes, we have simulated the Raman spectra using DFT; the results are shown in Figure S1. The precise wavenumbers for

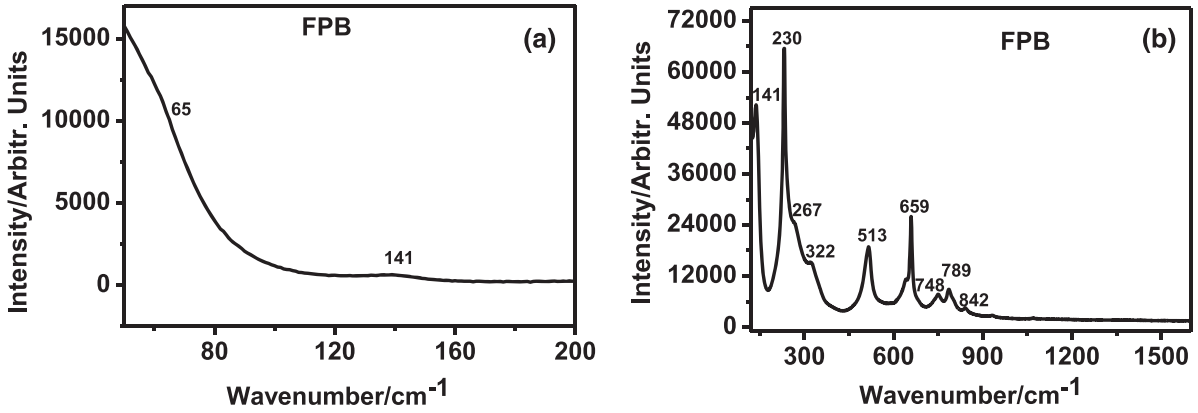

FIGURE 5 Raman spectra of FPB in the (a) low- and (b) medium-wavenumber region

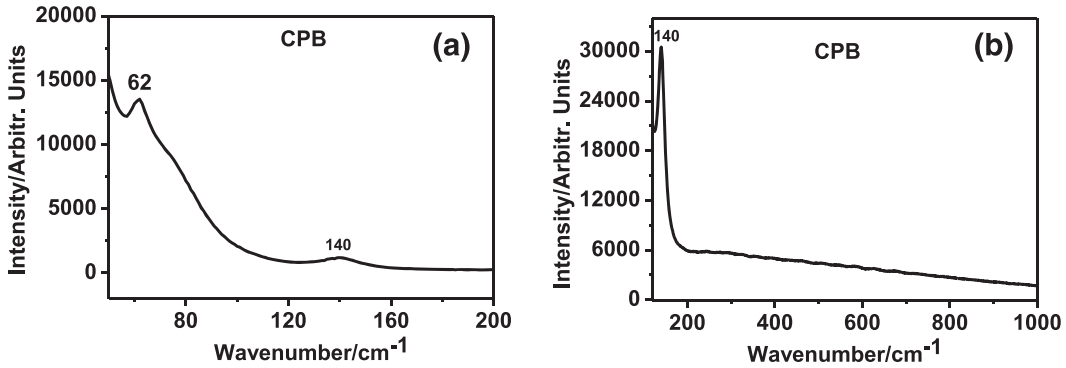

FIGURE 6 Raman spectra of CPB in the (a) low- and (b) medium-wavenumber region

individual modes have been summarized in Table S2. The simulated Raman spectra can only approximately reproduce the experimental results since we have dealt with only $MABr_3$. The spectral contribution related to the cations (FA, MA, and Cs) and their interactions with the anion Br^- is visible in the simulated spectra. The calculated Raman modes for the isolated parts of each material help to identify the vibrational modes originating from the lattice structure. We can assign the Raman modes around 420 and 442 cm^{-1} to the NH_2-C-NH_2 torsional motion.[24] Our calculations also reveal a mode for this motion at 490 cm^{-1} as shown in Table S2. The band at 1578 cm^{-1} could be assigned to the umbrella bending of NH_3. The scissoring vibration of NH_2 is reflected by the bands at 1628 and 1690 cm^{-1}. The simulated results also show vibrational modes from 3000 to 3600 cm^{-1}, which are due to the NH_2, NH_3, and CH_3 vibrations.

In a similar way, we have investigated FPB (Figure 5), in which only the cation is different in comparison to MPB. Like in MPB (see discussion above), the band found at 65 cm^{-1} is due to the bending mode of the Pb-Br-Pb bonds. The band at 141 cm^{-1} is due to the libration of the cations, which arises from the deformation of the inorganic cage. It is important to note that in both MPB and FPB, this band is broader than in CPB, which basically reflects the low octahedral activity of MPB and FPB compared to CPB. The larger Goldschmidt Tolerance Factor (GTF) of FA^+ and MA^+ compared to Cs^+ ensures the better fit of FA^+ and MA^+ to the octahedral cage and therefore a less flexible lattice.[26] The vibrational modes at 306 and 479 cm^{-1} are due to the out-of-plane symmetric and bending vibrations of the NH-C-NH bonds and the NH_2-C-NH_2 wagging motion, respectively. The vibrational mode at 746 cm^{-1} is assigned to the NH_2 torsional motion and the C-H out-of-plane bending, which is also observed in the simulation. The vibrational modes at around 1733 and 1788 cm^{-1} are assigned to the NH_2 scissoring motion. These results also correlate with previously reported data.[50,51]

Since CPB does not have any organic counterpart in the structure, we have only seen the vibrational modes associated with the $PbBr_6$ cage (Figure 6). Similar to MPB and CPB, the band detected at 65 cm^{-1} is due to the bending mode of the Br-Pb-Br bonds. The band at

141 cm^{-1} is due to the libration of the cations related to the deformation of the inorganic cage. The simulation produces several bands in the low-wavenumber region, which have been listed in Table S4.

When comparing the different materials, we observe that the associated Raman modes for FA^+ are shifted to higher wavenumbers compared to MA^+. The main reason for this is the weaker ionic bonding between FA^+ and Br^- because FA^+ has a weaker polarization and larger size than MA^+.[26] This can be further demonstrated by the electrostatic potential map (ESP), which yields the charge distribution of FA^+ and MA^+ and the extent of the interaction with Br^-. Figure 7a,b shows the ESPs of FA^+ and MA^+, respectively. The red parts show the electron-rich region and the blue parts show electron-poor regions. As mentioned above, MA^+ is more polarized than FA^+. In the FA^+ ion, the positive charge is delocalized between the two nitrogen atoms, whereas for MA^+ the electrons are localized on the nitrogen atom of the NH_3^+ ion. According to our theoretical calculations, FA^+ possesses a much lower dipole moment (0.28 D) than MA^+ (2.37 D). The weaker polarization and planar structure of FA^+ results in an out-of-plane vibration without significant interactions with the surrounding sublattice PbX_6.[26,52] Figure 7c–e show the ESPs of the interactions between MA^+, FA^+, and Cs^+ with Br^-, respectively. One finds that Cs^+ more strongly binds with Br^- than MA^+ and FA^+.

We have performed a band-profile analysis using a traditional deconvolution process over the whole range; details have been described earlier.[53] The experimental data have been analysed using pseudo-Voigt functions,

$$y = y_0 + A\left\{\mu\left(\frac{2}{\pi}\right)\left(\frac{w}{4(x-xc)^2+w^2}\right) + (1-\mu)\sqrt{\frac{4\ln(2)}{w\sqrt{\pi}}}\exp\left[-\left(\frac{4\ln(2)(x-xc)^2}{w^2}\right)\right]\right\}$$

where y_0 is an offset, μ is the profile shape factor, w the full width at half maximum (FWHM), and xc the line position. Varying the parameters, we have obtained quasi-Lorentzian profiles for all bands. The fitted curves and the deconvolution components of the Raman spectra for MPB and FPB are shown in Figure 8. Among all the extracted parameters, we have only focused on the FWHM of different components, which are listed in Tables 1 and 2 for two different perovskites. As the CPB does not show any vibrational features after 200 cm^{-1}, we did not attempt a deconvolution process there. The fitted curves and the deconvolution components of the Raman spectra below 200 cm^{-1} for MPB, FPB, and CPB are shown in Figure S3.

From the deconvolution analysis we find that the FWHM values differ for different bands. For example, we can focus on the NH_2 scissoring motion found at 1628 and 1688 cm^{-1} for MPB and at 1734 and 1788 cm^{-1} for

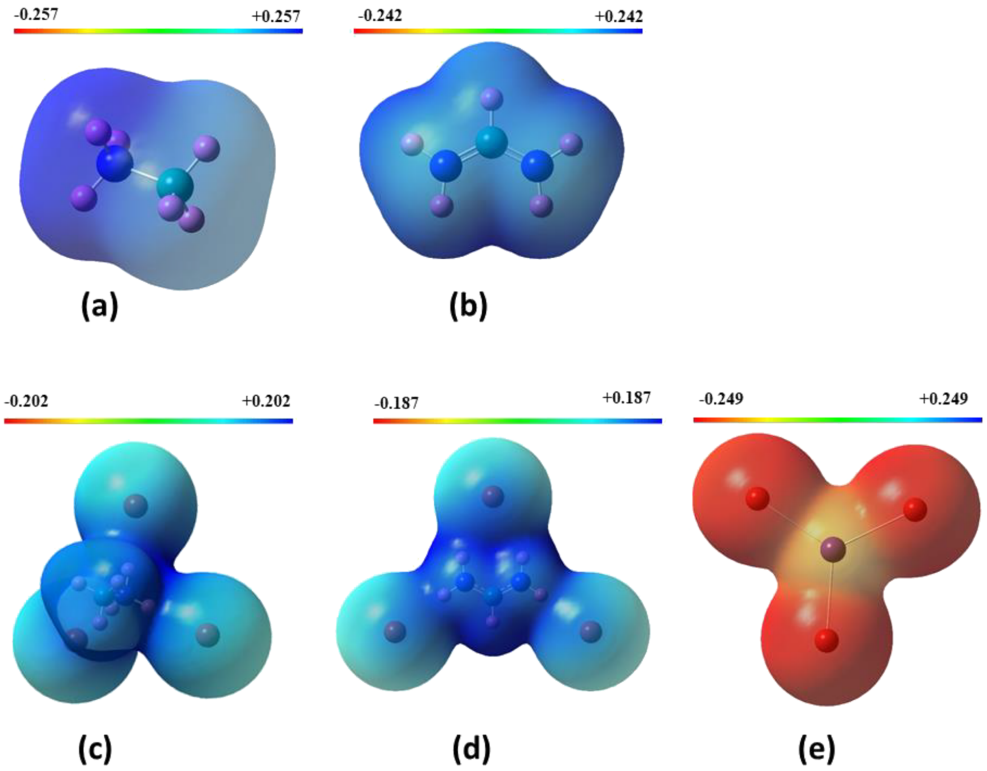

FIGURE 7 Electrostatic potential maps (ESPs) of the isolated parts of MPB, FPB, and CPB. (a) MA^+, (b) FA^+, (c) $MABr_3$, (d) $FABr_3$, and (e) $CsBr_3$

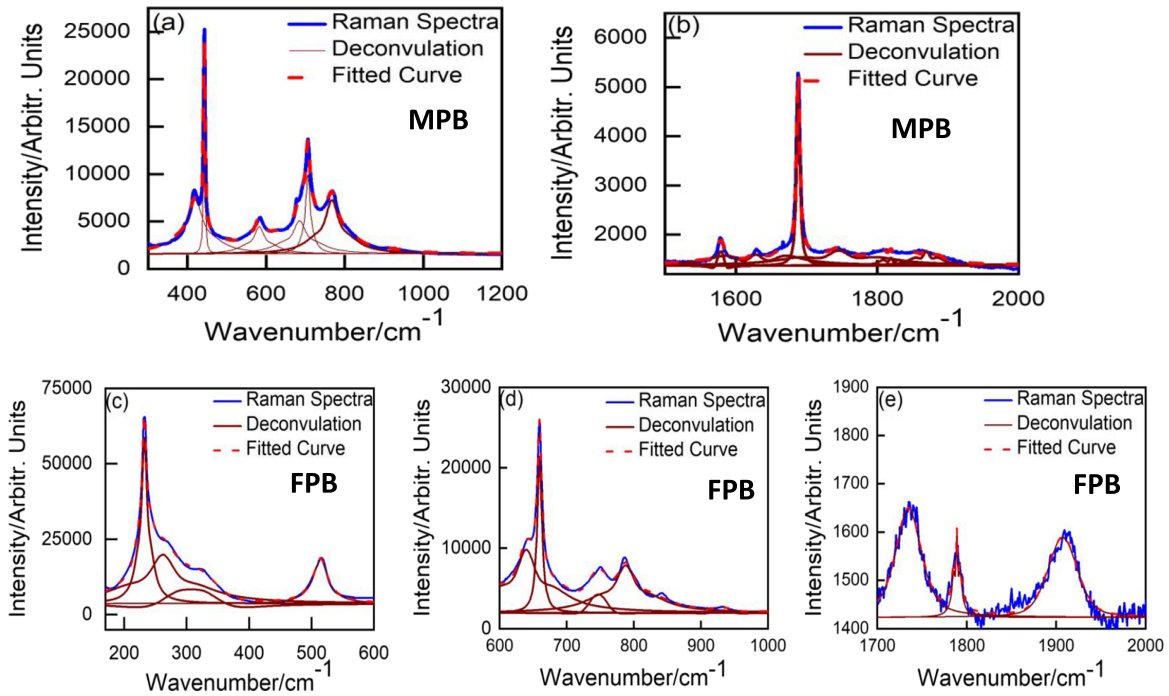

FIGURE 8 Fitted Raman spectra of (a and b) $MAPbBr_3$ and (c–e) $FAPbBr_3$ obtained with 785 nm excitation. The blue curves are used for the experimental Raman spectra, the red dotted lines show the cumulative fitting curve and the brown curves represent the deconvolution components

TABLE 1 Deconvolution analysis of different Raman bands in $MAPbBr_3$

No.	Peak position/cm^{-1}	FWHM/cm^{-1}
1	420	55
2	442	3.9
3	582	39
4	685	50
5	706	15
6	767	50
7	927	11
8	1578	10
9	1628	45
10	1688	5
11	1745	59
12	1819	11
13	1869	18

Abbreviation: FWHM, full width at half maximum.

TABLE 2 Deconvolution analysis of different Raman bands in $FAPbBr_3$

No.	Peak position/cm^{-1}	FWHM/cm^{-1}
1	232	12
2	261	64
3	306	75
4	514	28
5	640	46
6	660	8
7	746	31
8	788	31
9	842	17
10	1734	34
11	1788	3.8
12	1907	39

Abbreviation: FWHM, full width at half maximum.

FPB. We find that the FWHM values are smaller for FPB compared to MPB, which implies that the cation influences the line-width broadening of the Raman bands. In parallel, we see that the peak positions are also shifted for different cationic features.

The change of the polarizability of the cations and consequently the change of the extent of their interaction with other atoms, leads to the shift of Raman bands. This reflects the structural change, which becomes apparent when comparing the perovskites with different cations. It is important to note that from an XRD study one can

extract the structure of crystalline materials.[54,55] XRD is useful to quantify the atomic level distances, extract symmetries, compositional and temperature dependent phase orientation and size of crystallites in polycrystalline films.[56,57] On the other hand, Raman spectroscopy does not only provide information about chemical composition and phases in crystalline systems, but also can be used for the characterization of vibrational properties of amorphous structures, molecular materials, solvents, and gases.[58–60] It is also a useful tool for the investigation of the lattice vibration symmetry, degree of crystallinity, the structural change in mixed halide perovskites, electron–phonon interactions, dielectric screening, elastic properties and the stability of MHP during their operation in solar cell.[61,62]

5 | CONCLUSION

In summary, we have reported the vibrational properties of lead halide-based perovskites with different cation substitutions using Raman spectroscopy and density functional theory (DFT). We have experimentally observed the low- and medium-wavenumber Raman modes of these systems. Theoretical simulations resulted in more details regarding different modes of the isolated parts of the materials. This study provides insight into the polarizabilities of the isolated cations and the extent of their interactions with anions. We have found that when different cations are introduced, clear shifts of vibrational modes can be observed for the three different perovskite materials considered here. These shifts together with the broadening of the Raman bands reveal structural differences. Our study provides assignments of the different bands observed in the Raman spectra of MHP perovskites with different cations, which is an important information helping also other researchers to better understand fundamental properties of this class of materials in relation to their efficiency in optoelectronic devices.

ACKNOWLEDGEMENTS

S. G. is thankful to the Alexander von Humboldt-Stiftung, (Ref 3.5 - 1205997 - IND - HFST-P, AvH Foundation Germany), for the award of a postdoctoral fellowship and financial support. J.H. acknowledges financial support from the Research Foundation-Flanders (Fonds Wetenschappelijk Onderzoek, FWO, Grant Nos. G0A5817N, G098319N, W002221N, S002019N, and ZW15_09-G0H6316N), the Vlaamse regering through long-term structural funding Methusalem (CASAS2, Meth/15/04), the Onderzoeksraad, KU Leuven Research Fund (iBOF-21-085 PERSIST), and the Max-Planck-Gesellschaft as MPI fellow. B. P acknowledges a postdoctoral fellowship from the Research Foundation-Flanders (FWO Grant No. 1275521N).

ORCID

Supriya Ghosh https://orcid.org/0000-0002-5324-1583
Debkumar Rana https://orcid.org/0000-0001-8165-3289
Bapi Pradhan https://orcid.org/0000-0002-6202-7343
Patrice Donfack https://orcid.org/0000-0002-6120-4686
Johan Hofkens https://orcid.org/0000-0002-9101-0567
Arnulf Materny https://orcid.org/0000-0003-4707-195X

REFERENCES

[1] J. S. Manser, J. A. Christians, P. V. Kamat, *Chem. Rev.* **2016**, *116*, 12956.
[2] Q. Lin, Z. Wang, H. J. Snaith, M. B. Johnston, L. M. Herz, *Adv. Sci.* **2018**, *5*, 1700792.
[3] K. Lin, J. Xing, L. N. Quan, F. P. G. de Arquer, X. Gong, J. Lu, L. Xie, W. Zhao, D. Zhang, C. Yan, *Nature* **2018**, *562*, 245.
[4] Q. Shi, S. Ghosh, A. S. Sarkar, P. Kumar, Z. Wang, S. K. Pal, T. N. Pullerits, K. J. Karki, *J. Phys. Chem. C* **2018**, *122*, 3818.
[5] S. Ghosh, R. Ray, S. K. Pal, *J. Phys. Chem. C* **2021**, *125*, 3198.
[6] S. Ghosh, B. Pradhan, Y. Zhang, J. Hofkens, K. J. Karki, A. Materny, *Phys. Chem. Chem. Phys.* **2021**, *23*, 3983
[7] J. Huang, Y. Yuan, Y. Shao, Y. Yan, *Nat. Rev. Mater.* **2017**, *2*, 1.
[8] M. M. Lee, J. Teuscher, T. Miyasaka, T. N. Murakami, H. J. Snaith, *Science* **2012**, *338*, 643, 1228604.
[9] F. Deschler, M. Price, S. Pathak, L. E. Klintberg, D.-D. Jarausch, R. Higler, S. Hüttner, T. Leijtens, S. D. Stranks, H. J. Snaith, *J. Phys. Chem. Lett.* **2014**, *5*, 1421.
[10] I. Levchuk, A. Osvet, X. Tang, M. Brandl, J. D. Perea, F. Hoegl, G. J. Matt, R. Hock, M. Batentschuk, C. J. Brabec, *Nano Lett.* **2017**, *17*, 2765.
[11] L. Protesescu, S. Yakunin, M. I. Bodnarchuk, F. Bertolotti, N. Masciocchi, A. Guagliardi, M. V. Kovalenko, *J. Am. Chem. Soc.* **2016**, *138*, 14202.
[12] R. Ray, N. Nakka, S. K. Pal, *Nanotechnology* **2021**, *32*, 085201.
[13] X. Yu, T. Shen, C. Zhu, Q. Zeng, A. Yu, S. Liu, R. Yi, Z. Weng, Y. Zhan, X. Hou, J. Qin, *Nano Mater.* **2020**, *3*, 11889.
[14] W. S. Yang, J. H. Noh, N. J. Jeon, Y. C. Kim, S. Ryu, J. Seo, S. I. Seok, *Science* **2015**, *348*, 1234.
[15] M. Saliba, T. Matsui, J.-Y. Seo, K. Domanski, J.-P. Correa-Baena, M. K. Nazeeruddin, S. M. Zakeeruddin, W. Tress, A. Abate, A. Hagfeldt, *Energ. Environ. Sci.* **2016**, *9*, 1989.
[16] N. J. Jeon, J. H. Noh, W. S. Yang, Y. C. Kim, S. Ryu, J. Seo, S. I. Seok, *Nature* **2015**, *517*, 476.
[17] H. Zhou, Q. Chen, G. Li, S. Luo, T.-b. Song, H.-S. Duan, Z. Hong, J. You, Y. Liu, Y. Yang, *Science* **2014**, *345*, 542.
[18] S. Ghosh, S. K. Pal, K. J. Karki, T. Pullerits, *ACS Energy Lett.* **2017**, *2*, 2133.
[19] S. Ghosh, Q. Shi, B. Pradhan, P. Kumar, Z. Wang, S. Acharya, S. K. Pal, T. Pullerits, K. J. Karki, *J. Phys. Chem. Lett.* **2018**, *9*, 4245.
[20] V. D'Innocenzo, A. R. Srimath Kandada, M. De Bastiani, M. Gandini, A. Petrozza, *J. Am. Chem. Soc.* **2014**, *136*, 17730.
[21] T. Glaser, C. Müller, M. Sendner, C. Krekeler, O. E. Semonin, T. D. Hull, O. Yaffe, J. S. Owen, W. Kowalsky, A. Pucci, *J. Phys. Chem. Lett.* **2015**, *6*, 2913.

[22] M. A. Pérez-Osorio, R. L. Milot, M. R. Filip, J. B. Patel, L. M. Herz, M. B. Johnston, F. Giustino, *J. Phys. Chem. C* **2015**, *119*, 25703.
[23] G. T. Schuck, D. M. Többens, M. Koch-Müller, I. Efthimiopoulos, S. Schorr, *J. Phys. Chem. C* **2018**, *122*, 5227.
[24] C. Quarti, G. Grancini, E. Mosconi, P. Bruno, J. M. Ball, M. M. Lee, H. J. Snaith, A. Petrozza, F. De Angelis, *J. Phys. Chem. Lett.* **2013**, *5*, 279.
[25] R. G. Niemann, A. G. Kontos, D. Palles, E. I. Kamitsos, A. Kaltzoglou, F. Brivio, P. Falaras, P. J. Cameron, *J. Phys. Chem. C* **2016**, *120*, 2509.
[26] J. Ibaceta-Jaña, R. Muydinov, P. Rosado, H. Mirhosseini, M. Chugh, O. Nazarenko, D. N. Dirin, D. Heinrich, M. R. Wagner, T. D. Kühne, *Phys. Chem. Chem. Phys.* **2020**, *22*, 5604.
[27] T. Ivanovska, C. Quarti, G. Grancini, A. Petrozza, F. De Angelis, A. Milani, G. Ruani, *ChemSusChem* **2016**, *9*, 2994.
[28] K. Nakada, Y. Matsumoto, Y. Shimoi, K. Yamada, Y. Furukawa, *Molecules* **2019**, *24*, 626.
[29] J. A. Steele, P. Puech, M. Keshavarz, R. Yang, S. Banerjee, E. Debroye, C. W. Kim, H. Yuan, N. H. Heo, J. Vanacken, *ACS Nano* **2018**, *12*, 8081.
[30] J. A. Steele, H. Yuan, C. Y. Tan, M. Keshavarz, C. Steuwe, M. B. Roeffaers, J. Hofkens, *ACS Nano* **2017**, *11*, 8072.
[31] K. Zheng, T. Pullerits, *J. Phys. Chem. Lett.* **2019**, *10*, 5881.
[32] R. K. Misra, S. Aharon, B. Li, D. Mogilyansky, I. Visoly-Fisher, L. Etgar, E. A. Katz, *J. Phys. Chem. Lett.* **2015**, *6*, 326.
[33] S. Ghosh, Q. Shi, B. Pradhan, A. Mushtaq, S. Acharya, K. J. Karki, T. Pullerits, S. K. Pal, *J. Phys. Chem. Lett.* **2020**, *11*, 1239.
[34] J. W. Lee, D. J. Seol, A. N. Cho, N. G. Park, *Adv. Mater.* **2014**, *26*, 4991.
[35] Z. Yang, A. Surrente, K. Galkowski, A. Miyata, O. Portugall, R. J. Sutton, A. A. Haghighirad, H. J. Snaith, D. K. Maude, P. Plochocka, R. J. Nicholas, *ACS Energy Lett.* **2017**, *2*, 1621.
[36] E. Mosconi, D. Meggiolaro, H. J. Snaith, S. D. Stranks, F. De Angelis, *Energy Environ. Sci.* **2016**, *9*, 3180.
[37] K. Zheng, Q. Zhu, M. Abdellah, M. E. Messing, W. Zhang, A. Generalov, Y. Niu, L. Ribaud, S. E. Canton, T. Pullerits, *J. Phys. Chem. Lett.* **2015**, *6*, 2969.
[38] S. Colella, E. Mosconi, P. Fedeli, A. Listorti, F. Gazza, F. Orlandi, P. Ferro, T. Besagni, A. Rizzo, G. Calestani, *Chem. Mater.* **2013**, *25*, 4613.
[39] B. Wu, H. Yuan, Q. Xu, J. A. Steele, D. Giovanni, P. Puech, J. Fu, Y. F. Ng, N. F. Jamaludin, A. Solanki, *Nat. Commun.* **2019**, *10*, 1.
[40] D. A. Long, The Raman Effect, John Wiley & Sons Ltd, Chichester, **2002**
[41] H. Edwards, *J. Raman Spectrosc.* **1995**, *26*, 587.
[42] N. Giesbrecht, J. Schlipf, L. Oesinghaus, A. Binek, T. Bein, P. Müller-Buschbaum, P. Docampo, *ACS Energy Lett.* **2016**, *1*, 150.
[43] F. Zhang, B. Yang, K. Zheng, S. Yang, Y. Li, W. Deng, R. He, *Nano Lett.* **2018**, *10*, 1.
[44] M. J. Frisch, G. W. Trucks, H. B. Schlegel, G. E. Scuseria, M. A. Robb, J. R. Cheeseman, G. Scalmani, V. Barone, B. Mennucci, G. A. Petersson, H. Nakatsuji, M. Caricato, X. Li, H. P. Hratchian, A. F. Izmaylov, J. Bloino, G. Zheng, J. L. Sonnenberg, M. Hada, M. Ehara, K. Toyota, R. Fukuda, J. Hasegawa, M. Ishida, T. Nakajima, Y. Honda, O. Kitao, H. Nakai, T. Vreven Jr., J. A. Montgomery, J. E. Peralta, F. Ogliaro, M. Bearpark, J. J. Heyd, E. Brothers, K. N. Kudin, V. N. Staroverov, R. Kobayashi, J. Normand, K. Raghavachari, A. Rendell, J. C. Burant, S. S. Iyengar, J. Tomasi, M. Cossi, N. Rega, N. J. Millam, M. Klene, J. E. Knox, J. B. Cross, V. Bakken, C. Adamo, J. Jaramillo, R. Gomperts, R. E. Stratmann, O. Yazyev, A. J. Austin, R. Cammi, C. Pomelli, J. W. Ochterski, R. L. Martin, K. Morokuma, V. G. Zakrzewski, G. A. Voth, P. Salvador, J. J. Dannenberg, S. Dapprich, A. D. Daniels, Ö. Farkas, J. B. Foresman, J. V. Ortiz, J. Cioslowski, D. J. Fox, *F. Gaussian 09 Revision A.1*, Gaussian, Inc., Wallingford CT **2009**.
[45] R. Dennington, T. Keith, J. Millam, *GaussView (Version 5)*, Semichem, Inc., Shawnee Mission, KS **2009**.
[46] Q. Shi, S. Ghosh, P. Kumar, L. C. Folkers, S. K. Pal, T. N. Pullerits, K. J. Karki, *J. Phys. Chem. C* **2018**, *122*, 21817.
[47] K. Zheng, K. Žídek, M. Abdellah, M. E. Messing, M. J. Al-Marri, T. Pullerits, *J. Phys. Chem. C* **2016**, *120*, 3077.
[48] G. Mannino, I. Deretzis, E. Smecca, A. La Magna, A. Alberti, D. Ceratti, D. Cahen, *J. Phys. Chem. Lett.* **2020**, *11*, 2490.
[49] A. M. Leguy, A. R. Goñi, J. M. Frost, J. Skelton, F. Brivio, X. Rodríguez-Martínez, O. J. Weber, A. Pallipurath, M. I. Alonso, M. Campoy-Quiles, *Phys. Chem. Chem. Phys.* **2016**, *18*, 27051.
[50] L. Wang, K. Wang, B. Zou, *J. Phys. Chem. Lett.* **2016**, *7*, 2556.
[51] E. Kucharska, J. Hanuza, A. Ciupa, M. Mączka, L. Macalik, *Vib. Spectrosc.* **2014**, *75*, 45.
[52] A. A. Petrov, E. A. Goodilin, A. B. Tarasov, V. A. Lazarenko, P. V. Dorovatovskii, V. N. Khrustalev, *Acta Crystallogr. E* **2017**, *73*, 569.
[53] S. Kuznetsov, V. Novikov, E. Sagitova, L. Y. Ustynyuk, A. Glikin, K. Prokhorov, G. Y. Nikolaeva, P. Pashinin, *Laser Phys.* **2019**, *29*, 085701.
[54] B. Warren, B. Averbach, *J. Appl. Phys.* **1952**, *23*, 497.
[55] J. Rivnay, R. Noriega, R. J. Kline, A. Salleo, M. F. Toney, *Phys. Rev. B* **2011**, *84*, 045203.
[56] S. Ruddlesden, P. Popper, *Acta Crystallogr.* **1958**, *11*, 54.
[57] P. Whitfield, N. Herron, W. Guise, K. Page, Y. Cheng, I. Milas, M. Crawford, *Sci. Rep.* **2016**, *6*, 1.
[58] M. Iliev, M. Abrashev, J. Laverdiere, S. Jandl, M. Gospodinov, Y.-Q. Wang, Y.-Y. Sun, *Phys. Rev. B* **2006**, *73*, 064302.
[59] D. K. Pandey, P. Sanchora, D. Rana, P. Donfack, A. Materny, D. K. Singh, *J. Raman Spectrosc.* **2020**, *51*, 147.
[60] S. Falke, P. Eravuchira, A. Materny, C. Lienau, *J. Raman Spectrosc.* **2011**, *42*, 1897.
[61] G. Abdelmageed, L. Jewell, K. Hellier, L. Seymour, B. Luo, F. Bridges, J. Z. Zhang, S. Carter, *Appl. Phys. Lett.* **2016**, *109*, 233905.
[62] A. Létoublon, S. Paofai, B. Ruffle, P. Bourges, B. Hehlen, T. Michel, C. Ecolivet, O. Durand, S. Cordier, C. Katan, *J. Phys. Chem. Lett.* **2016**, *7*, 3776.

SUPPORTING INFORMATION

Additional supporting information may be found online in the Supporting Information section at the end of this article.

How to cite this article: S. Ghosh, D. Rana, B. Pradhan, P. Donfack, J. Hofkens, A. Materny, *J Raman Spectrosc* **2021**, *52*(12), 2338. https://doi.org/10.1002/jrs.6141